Solar Energy Materials & Solar Cells 273 (2024) 112940

Contents lists available at ScienceDirect

Solar Energy Materials and Solar Cells

journal homepage: www.elsevier.com/locate/solmat

Enhanced visible light-activated gas sensing properties of nanoporous copper oxide thin films

Andrzej Kwiatkowski [a], Janusz Smulko [a,*], Katarzyna Drozdowska [a], Lars Österlund [b], Tesfalem Welearegay [b,**]

[a] Department of Metrology and Optoelectronics, Faculty of Electronics, Telecommunications, and Informatics, Gdańsk University of Technology, G. Narutowicza 11/12, 80-233, Gdańsk, Poland

[b] Department of Materials Science and Engineering, The Ångström Laboratory, Uppsala University, P.O. Box 35, SE-75103, Uppsala, Sweden

ARTICLE INFO

Keywords:
Chemical sensor
Gas sensing
Nanoporous CuO
Temperature modulation
Light activation

ABSTRACT

Metal oxide gas sensors are popular chemoresistive sensors. They are used for numerous tasks, including environmental and safety monitoring. Some gas-sensing materials exhibit photo-induced properties that can be utilized for enhanced gas detection by modifying the sensor selectivity and sensitivity when illuminated by light. Here, we present the gas sensing characteristics of highly nanoporous Cu_2O thin films towards both electrophilic (NO_2) and nucleophilic (C_2H_5OH, NH_3) gas molecules under ambient temperature and modulated by visible light illumination of different colors (red: 632 nm, green: 530 nm, blue: 468 nm). Cu_2O films were fabricated by reactive advanced gas deposition (AGD) technology. The surface and structural analysis of the samples confirm the deposition of nanoporous thin films of mixed copper oxide phases. The gas sensing property of Cu_2O exhibited expected *p*-type semiconductor behavior upon electrophilic and nucleophilic gas exposures. Our results show that visible light illumination provides enhanced sensor response.

1. Introduction

Metal oxide gas sensors (MOx) require continuous development due to emerging applications in medical diagnostics, industrial processes, environmental monitoring, and security [1–3]. We need low-cost and highly accurate gas sensors for almost everyday applications to determine the composition of gas mixtures in practical conditions. Despite known disadvantages such as limited selectivity, repeatability, and drifts, chemoresistive gas sensors are of central interest in this area [4, 5]. These sensors have profound benefits, including low manufacturing costs and relatively simple electronic systems for data acquisition. A voltage divider, comparator, or analog-to-digital converter built into microcontrollers can be used in the most straightforward practical implementations of electronic circuits utilizing resistive gas sensors. Moreover, these gas sensors can be modulated to enhance gas selectivity and sensitivity by modifying their operating temperature or applying light illumination in the case of photo-active sensor materials, heterostructures, or nanostructures of different morphologies, demonstrating enhanced gas selectivity and reducing cross-sensitivity to ambient gases [6–9]. In fact, many materials applied in various fields of solar energy technology are also suitable as photo-activated gas sensors, as noted in the book by Smith and Granqvist [10]. The applied microcontroller determines the modulation and reduces the required gas sensors necessary for detecting gas mixtures of interest. Such advanced schemes to modulate sensor responses provide means to lower maintenance costs and lower total energy consumption. The applied microcontroller can also run data processing (detection algorithms, drift removal, etc.) to improve sensor efficiency [11–14].

Various approaches have also been introduced to enhance resistive gas sensors' response by employing heterostructure materials, different morphologies, and doping with noble metals [15–18]. However, there is an enormous need for further enhancement techniques. Due to their simplicity, low operating temperature, and low surface resistance – metal oxide gas sensors based on *p*-type semiconductor nanostructures have recently been identified as promising materials in gas sensor technology [19]. Although the relative sensor responses of *p*-type MOx

* Corresponding author. Department of Metrology and Optoelectronics, Faculty of Electronics, Telecommunications, and Informatics, Gdańsk University of Technology, G. Narutowicza 11/12, 80-233, Gdańsk, Poland.

** Corresponding author. Department of Materials Science and Engineering, The Ångström Laboratory, Uppsala University, 75103, Uppsala, Sweden.

E-mail addresses: janusz.smulko@pg.edu.pl (J. Smulko), tesfalem.welearegay@angstrom.uu.se (T. Welearegay).

https://doi.org/10.1016/j.solmat.2024.112940

Received 5 January 2024; Received in revised form 3 April 2024; Accepted 14 May 2024

Available online 17 May 2024

are lower than that of *n*-type, their different affinity towards electrophilic and nucleophilic molecules and their generally lower sensitivity towards humidity make them excellent alternatives, or complements, to *n*-type MOx operating at high temperatures.

This article presents a gas sensor utilizing a nanoporous copper oxide (Cu_2O) film, which has been identified as an interesting material for gas sensing [20]. Cu_2O nanostructures are *p*-type metal oxide semiconductors, and their conductivity is attributed to copper vacancies inside the network structure, with electronic bandgap ranging between 1.2 and 1.9 eV, i.e., 1033 nm–653 nm [21]. Copper oxides exist in many phases: CuO: (tenorite), Cu_2O (cuprite), and Cu_4O_3 (paramelaconite). The growth process upon their formation during particle and film growth decides which phase forms the formation phase. Since Cu_2O absorbs visible light, its conductivity can be selectively modulated by light using a few different wavelengths (e.g., using an RGB LED, emitting red, green, and blue light of adjusted intensity, respectively). The physicochemical properties of copper oxide thin films prepared by chemical deposition depend strongly on annealing treatments [21,22]. Cu_xO is thus an attractive *p*-type metal oxide for chemoresistive and optical sensing applications, where it is interesting to explore different synthesis routes, nanostructure, and reaction conditions.

Herein, we report the fabrication and deposition of nanoporous Cu_2O for gas sensing applications employing a gas evaporation technique pioneered by Granqvist et al. [23] We report on the gas sensing property towards electrophilic (nitrogen dioxide, NO_2) and nucleophilic gases (ethanol, C_2H_5OH; ammonia, NH_3) at different substrate temperatures and visible light irradiation conditions. We unravel enhanced and selective sensor responses. Hence, the as-fabricated highly nanoporous Cu_2O-based gas sensor presents enhanced gas sensing characteristics at low operating temperatures under visible light illumination.

2. Experimental details

2.1. Material synthesis

Sensors samples based on nanoporous Cu_2O thin films were fabricated and deposited onto a 15 μm gapped platinum interdigitated electrode (IDE) structures printed on a ceramic substrate (TESLA BLATNÀ, a.s., Czech Republic) [24]. The single-step fabrication and deposition of the nanoporous Cu_xO thin films were performed using a reactive advanced gas deposition (AGD) technique (Ultra Fine particle Equipment, ULVAC Ltd., Japan) using high-purity metallic copper (purity, 99.999 %) as source material [23]. Briefly, the AGD apparatus comprises two stainless-steel chambers connected by a transfer pipe. The two chambers, the source chamber 1 and deposition chamber 2, are maintained at different vacuum pressures, P_1 and P_2, respectively, where $P_1 > P_2$. The principle of operation of AGD is based on accurate control of the partial pressure of the metal source by controlling the temperature of the target material, which is held close to its melting temperature, and simultaneously cooling the vaporized source material by injecting gas into the source chamber, thus inducing nucleation of the vaporized metal atoms. Reactive cooling is achieved by blending O_2 gas into the He flow, causing metal oxide particles to nucleate in the melt zone. The formed particles exhibit log-normal size distribution, with typical particle sizes in the range of 1–10 nm that can be reproducibly controlled by adjusting the partial pressure of the evaporated material. A 3 mm transfer pipe pumps the condensed particles to the deposition chamber, where they are deposited in a substrate, here the IDE substrate. A stream of nanoparticles impinges on the substrate mounted on an XYZ stage motor, resulting in the deposition of highly nanoporous films [25].

Specifically, Cu_2O sensor samples are here prepared by heating pellets of Cu metal in a graphite crucible (Almath Crucibles, Ltd., UK) with an induction power of 3.4 kW under a laminar He (purity, 99.997 %) and O_2 (purity 99.997 %) gases flow of 30 L/min and 0.1 L/min, respectively. Before the evaporation and deposition process, the chambers were initially pre-evacuated. The evaporation and deposition pressures were then adjusted to $P_1 = 200$ kPa and $P_2 = 0.6$ kPa, respectively. The IDE substrate mounted on the XYZ stage motor was moved at a speed of 2.5 mm/s that enabled uniform deposition of Cu_2O thin films over the sensing area of the IDE area on the substrates. The as-fabricated sensor samples were subsequently annealed ex vacuo at 300 °C overnight.

2.2. Structural characterization

The surface morphology and structure of Cu_2O thin films were investigated by scanning electron microscopy (SEM) using a Zeiss LEO 155 microscope. X-ray diffractogram (XRD) was acquired employing a Siemens D5000 diffractometer with $Cu_{\alpha I,II}$ radiation, $\lambda = 1.5418$ Å. Divergence and anti-scattering slits of 1° were used. Data were recorded for 2θ from 20° to 80° with a 0.02-degree step size. The average crystallite size was calculated from the average of multiple peaks using Scherrer analysis assuming spherical particle shape (shape factor 0.9). The surface elemental composition and oxidation state of the Cu_xO thin films were investigated by X-ray photoelectron spectroscopy (XPS) using an Ulvac PHI Quantera II instrument equipped with Al $K_{\alpha 1}$ source, and a low energy flood gun was employed for charge neutralization. Survey scans of the samples were acquired between 0 and 1100 eV, employing a pass energy of 224 eV and an energy resolution of 0.8 eV. High-resolution scans were measured at a pass energy of 55 eV with a 0.2 eV energy resolution. All XPS spectra were analyzed using CASA XPS software. The internal C1s sample peak defined to be at 284.8 eV was employed as a rough calibration of the binding energy [26], not performing any more rigorous energy calibration appropriate for insulating samples [27]. The latter is motivated by the good electrical conductivity across the measured films (≈30 Ω) and the application of flood gun neutralization with no significant differences in the C1s peak position (<0.1 eV) for any of the samples.

2.3. Measurement setup

The sensor measurement setup utilizes a voltage divider biased by a low-noise voltage source. The voltage source of 2.5 V (type REF192) was used with a precise voltage divider and voltage buffer based on low-noise operational amplifier MAX4478 to reduce the bias voltage to 0.1 V and the current through the investigated gas sensor. The output voltage of the measurement setup was recorded by a precise multimeter (Keithley 2002), controlled by homemade software. The sensor temperature was monitored by recording the resistance of the built-in temperature Pt1000 sensor on the ceramic sensor substrate. The sensors were placed inside a glass gas chamber (Fig. 1a) at the same distance of about 1 cm from the RGB LED light source.

The temperature of the gas-sensitive layer was adjusted by DC voltage supplied to the sensor's heater from a programmable power supplier (Keysight E3648A). Photo-activation of the Cu_2O layer was induced by applying adjusted optical powers and wavelengths of light. Here, an RGB LED (LL-509RGBC2E-006) light source was used. We used the same optical power of the light for available wavelengths (0.5 mW at a distance of approximately 1 cm from the sensor surface). Additionally, before the measurements, the glass gas chamber and PCB board were washed with isopropanol, dried, and then ventilated with synthetic air. The glass chamber was placed inside the stainless steel box to protect the sensors against external light sources.

3. Results and discussion

3.1. Structural and morphological characteristics of the sensor films

Nanoporous copper oxide thin films were directly deposited onto a few ceramic-based gas sensor substrates. The color of the as-deposited thin films was dark brownish, indicating partially reduced copper oxide. The thin films as-deposited copper oxide were then annealed at

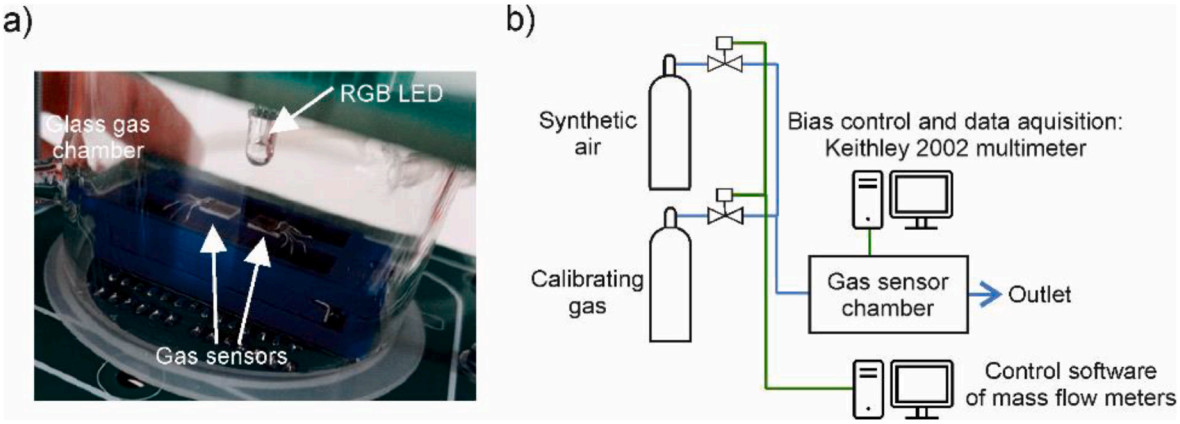

Fig. 1. The gas sensing measurement setup: a) gas chamber with a visible light source (RGB LED, type LL-509RGBC2E-006) and sensor samples, b) schematic drawing of the mass flow system setup for test gases (C_2H_5OH, NO_2, NH_3) diluted in synthetic air.

300 °C to remove carbon impurities from the surface. The surface morphology of the films depicted in Fig. 2 shows a porous surface characterized by ~100 nm size aggregates of Cu_2O nanoparticles with an average crystallite size of ≈5 nm as calculated from the Sherrer's formula. The porosity was estimated to be 53 %, with a broad pore size distribution around 30 nm. The geometrical surface area of the film, assuming cubic Cu_2O crystals, was then estimated to be about 400 m^2/g. We prepared a batch of samples of various thicknesses between 500 nm and 1500 nm. The sample with the most stable gas sensor response (the smallest drift in time) and DC resistance of about 30 Ω in the ambient atmosphere of synthetic air was selected for detailed studies reported here, and they were all 500 nm thick. The samples were experimentally studied a month after their preparation. It confirmed that within a month, the gas sensing layer had stable contact with the applied ceramic platform with the interdigitated platinum electrodes. Moreover, the gas response of the selected sample from the prepared batch results in repeatable measurement results within three weeks when the measurements were run. These results suggest a reasonable durability within at least several months.

The as-fabricated films were analyzed by XRD to investigate the crystallographic structure of Cu_xO surfaces. It can be inferred from Fig. 3, which shows a representative diffractogram of as-fabricated films, that the films exhibit sharp diffraction peaks characteristic of nanocrystalline oxygen-deficient copper oxide structures consisting of Cu_2O and minor amounts of Cu_4O_3 phase [28]. In particular, the diffractogram in Fig. 3 shows distinct and sharp peaks at 2θ = 36.7°, 42.7°,

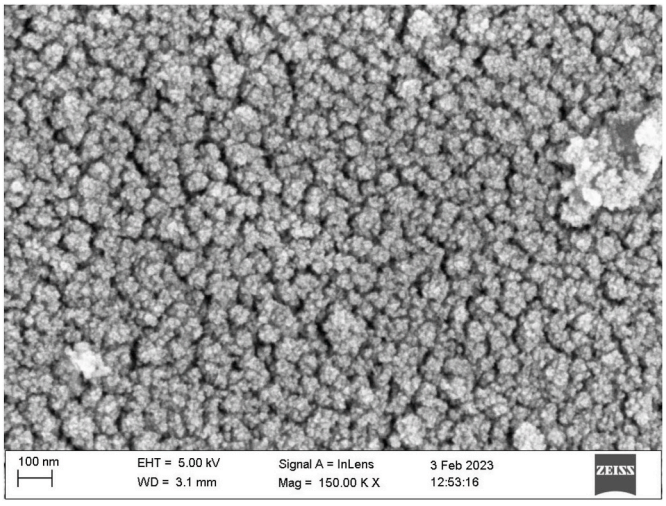

Fig. 2. SEM image of nanoporous Cu_2O thin film.

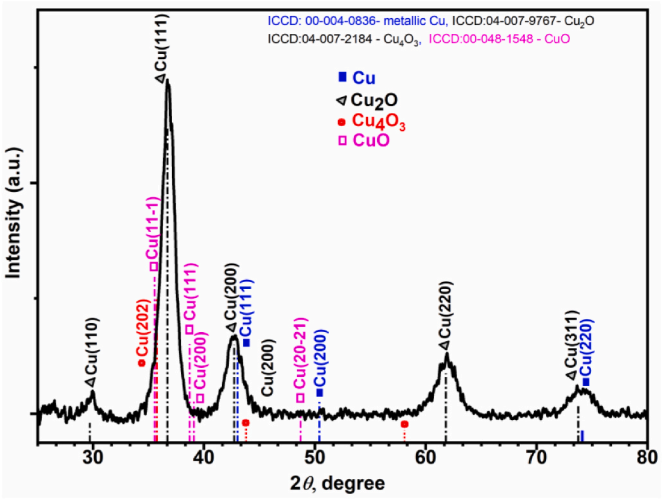

Fig. 3. XRD diffractogram recorded for as-prepared copper oxide thin film. Symbols and the corresponding ICCD numbers, shown in the figure legend, indicate reference peak positions.

and 61.8° with reflections associated with the (111), (200), and (211) crystal planes, respectively, corresponding to Cu_2O (ICCD: 04-007-9767). The presence of small amounts of tetragonal Cu_4O_3 may be discerned from the weak low-angle shoulder of the Cu_2O(111) peak, which can be ascribed to the Cu_4O_3(202) diffraction peaks at 2θ = 35.65° (ICCD: 04-007-2184), and the high-angle shoulder of the Cu_2O (200) peak at 2θ = 44.2° (ICCD: 04-007-2184). There is no evidence of detectable amounts of metallic Cu. Moreover, the absence of the high-intensity diffraction peak at 2θ = 38.7° corresponding to CuO(111) reflection planes (ICCD: 04-007-1548) shows that the sensor film does not contain CuO, which is indirectly also corroborated by the low film resistance (see below). We can thus conclude that the as-produced nanoporous copper oxide thin film is mainly dominated by Cu_2O with small amounts of Cu_4O_3 phase.

X-ray photon spectroscopy (XPS) studies of the as-fabricated nanoporous copper oxide thin films were conducted to investigate further the surface composition and oxidation state of the samples. A typical high-resolution XPS spectrum of copper oxide thin film in the Cu2p core level region is depicted in Fig. 4. The components were fitted using Gaussian-Lorenzian functions after Shirley background correction [29]. To elucidate the spin-spin splitting of the core level Cu2p and the corresponding oxidation states of copper, high-resolution Cu $2p_{3/2}$ spectra were deconvoluted into three components. The main peak at 932.6 eV

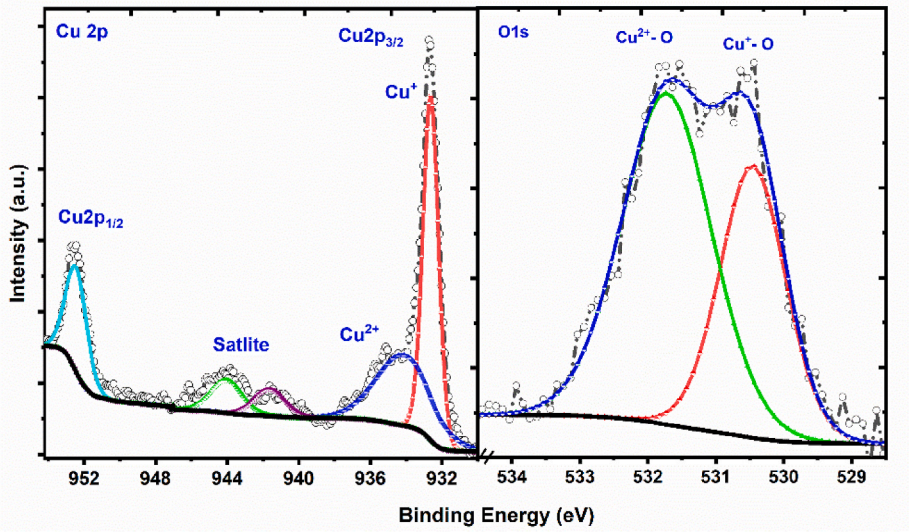

Fig. 4. XPS spectra of copper oxide in the Cu2p core level region (left) and O1s (right). The main peaks are due to Cu(I) (red line), while the Cu(II) band appears as high-energy shoulders (blue line).

corresponds to Cu^{+1} in the Cu_2O phase. The spectra of Cu2p exhibited characteristic spin-orbit splitting of 19.8 eV of the peaks due to Cu(I) at binding energies 932.6 eV ($2p_{3/2}$) and 952.4 eV ($2p_{1/2}$). The presence of a broad weak peak at 934.8 eV indicates the presence of Cu^{2+} ions, which we, based on our XRD analysis, attribute to a Cu_4O_3 phase [29]. It is important to note that the Cu_4O_3 phase contains both the Cu^{1+} and Cu^{2+} mixed valences, and thus, the as-prepared thin films contain both Cu^{1+} and Cu^{2+} [27,28,30].

The XPS spectra of O1s shown in Fig. 4 (right) depict a pronounced peak at 530.4 eV, which can be attributed to the O^{2-} ion in Cu_2O. A relatively strong intensity peak at a higher binding energy, 531.6 eV, also depicts the presence of another O^{2-} associated with higher copper oxidation states in the film, Cu(II). The observation that the detected Cu (II)/Cu(I) intensity ratio is higher in XPS compared with XRD can be explained by the surface sensitivity of XPS and an outermost oxidized copper surface. Thus, it is likely that the two O1s peaks are due to the presence of different copper oxides, Cu_2O and Cu_4O_3, as well as weak intensity contributions from surface hydroxyls readily adsorbed on the surface of the film, which also suggests the high porosity of the as-produced thin films. It is worth mentioning that thermal annealing of the films can drastically change their composition and structure. Hence, the high porosity of the film could also enhance the adsorption of high amounts of water. However, reports suggest that the growth orientation of the film is highly dependent on the substrate heating conditions during the deposition [31]. Copper oxide thin films as-deposited on unheated substrates are predominantly composed of Cu_2O, while films as-deposited on a heated substrate are reared to exhibit mainly CuO [31]. Notably, our AGD fabricated thin films were directly deposited on unheated substrates, and both XRD and XPS studies of the samples confirm the formation of Cu_2O with a smaller amount of a Cu_4O_3 phase at their surfaces.

3.2. Gas sensing characterization

The films' gas sensing properties were investigated towards electrophilic (NO_2) and nucleophilic (C_2H_5OH, NH_3) gases. The sensor's response was first analyzed by examining the impact of illuminating the sensing film at various visible light wavelengths. For this purpose, the sensor was illuminated with visible radiation at the following wavelengths: 632 nm (red), 530 nm (green), and 468 nm (blue), i.e., colors that all have larger energy than the reported bandgap of Cu_2O nanoparticles. The optical powers were adjusted to 0.5 mW in all cases.

Fig. 5 shows the relative change of the resistance when the sensor was exposed to pulses of ethanol vapor (140 ppm) diluted in synthetic air (S.A.) for 1 h. As expected, the resistivity increases in ethanol and ammonia gas since electrons are transferred from ethanol to the valence band of the *p*-type sensors, which results in the formation of electron-hole combinations and leading to the decrease in the total charge carrier hole density in the conduction channel, as exhibited by the decrease in measured conductance. Such time series of DC resistances were observed in several experiments during consecutive days. Moreover, all colors induce changes in the electrical properties, but the green and red color illumination leads to a large drift of sensor response. In contrast, blue light irradiation significantly improved the sensor's response and recovery time compared to non-illuminated conditions. At the same time, relative changes of DC resistance upon purging C_2H_5OH gas were similar for the three applied light irradiations for all wavelengths

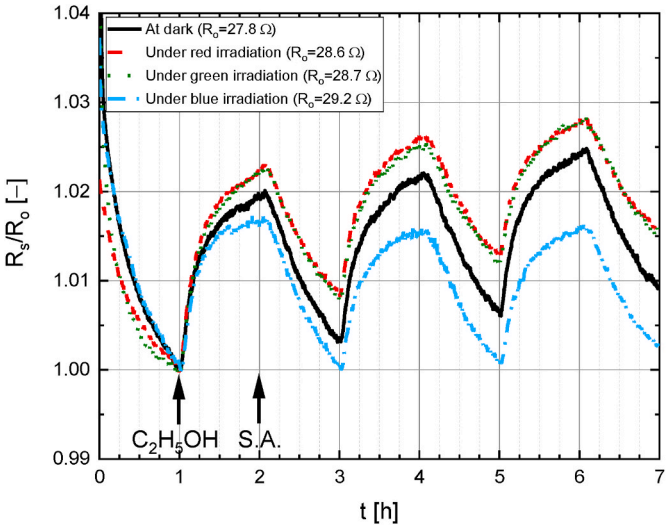

Fig. 5. Response of Cu_2O sensor towards 140 ppm ethanol (C_2H_5OH) gas in dark and under visible light irradiation of wavelengths: red (632 nm), green (520 nm), and blue (468 nm). The sensor's response was calculated as R_S/R_o, where R_S, R_o– denotes the sensor's resistance in the presence of target gas and/or visible light irradiation and the resistance under synthetic air (S.A.) exposure, respectively. An RGB LED, LL-509RGBC2E-006, with an optical power of 0.5 mW, was used for all wavelengths.

(Fig. 5). The photon-induced oxygen ions at the sensing surface can explain this effect. The shorter wavelength of blue light is above the bandgap energy of Cu_2O (about 2 eV) and generates electron-hole pairs that react with adsorbed molecules. Therefore, the gas response, induced by the electrons transferred from ethanol, is faster and does not include slow components, as observed in the dark.

The following experiments were performed to determine the optimal operating temperatures of the Cu_xO sensors. The sensor was placed in an ambient atmosphere by adding the selected gases in the dark and under blue light illumination. Further improvement in the sensor response was observed when the optical power was increased to its nominal value of 2.5 mW. Hence, the sensor's response to two gases of opposite chemical properties, reducing (NH_3) and oxidizing (NO_2), was studied at an optical power of 2.5 mW. The sensor's operating temperature was changed from 50 °C to 200 °C in consecutive steps of 10 °C every 10 min. The results, normalized to the sensor resistance recorded at 50 °C, observed in dark and under blue light irradiation, are presented in Figs. 6a and 7a, respectively. Further data processing was made by calculating the

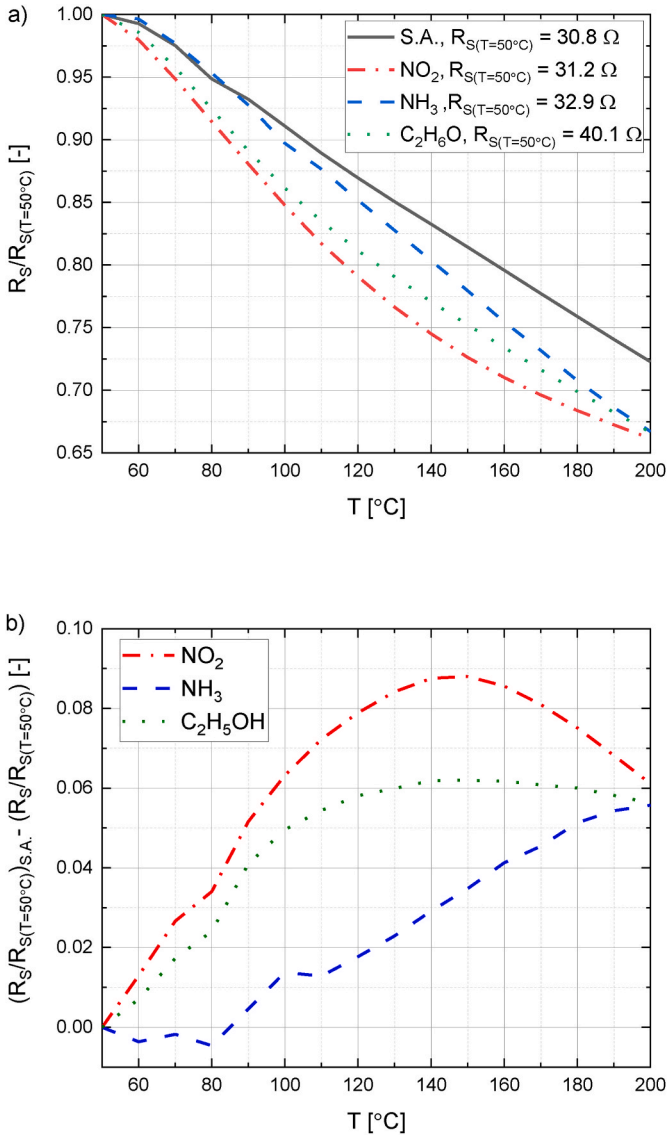

Fig. 6. Gas response of the Cu_xO sensor to 2 ppm NO_2, 10 ppm NH_3 and 140 ppm C_2H_5O gas exposures under dark conditions vs heating temperature T [°C]: a) R_S related to its resistance $R_{S(T\,=\,50°C)}$ at T = 50 °C, b) difference between the relative sensor resistance $(R_S/R_{S(T\,=\,50°C)})_{S.A.}$ in S.A. and relative resistance $(R_S/R_{S(T\,=\,50°C)})_{S.A.}$ upon gas exposure.

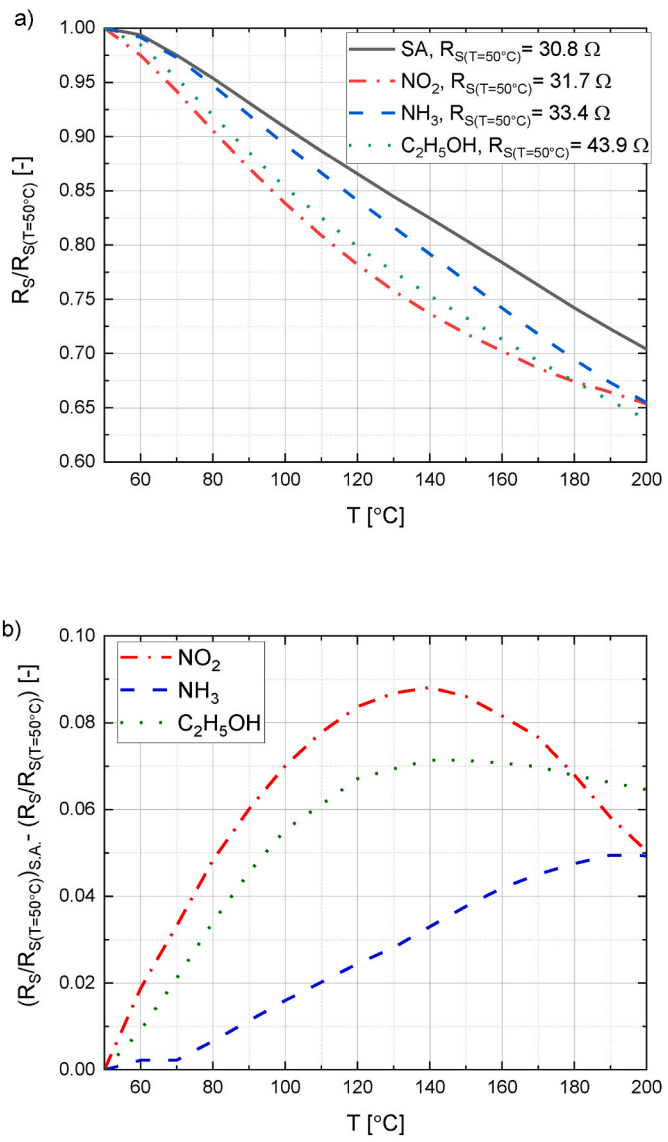

Fig. 7. Gas response of the Cu_xO sensor to 2 ppm NO_2, 10 ppm NH_3, and 140 ppm C_2H_5O gas exposures under blue light illumination vs heating temperature T [°C]: a) R_S related to its resistance $R_{S(T\,=\,50°C)}$ at T = 50 °C, b) difference between the relative sensor resistance $(R_S/R_{S(T\,=\,50°C)})_{S.A.}$ in S.A. and relative resistance $(R_S/R_{S(T\,=\,50°C)})_{S.A.}$ upon gas exposure.

difference between the sensor's response in the ambient atmosphere of the test gases (NH_3, NO_2, and C_2H_5OH) and the sensor's response to synthetic air alone (Figs. 6b and 7b). The latter comparison enabled better visualization of the recorded data. The location of the visible maxima allows us to determine the optimal temperature of the Cu_xO film for which the relative change in resistance for the considered gases has the highest value. Comparing Figs. 6b and 7b, it can be seen that upon blue light illumination, the sensor's operating temperature is reduced by about 10 °C for NO_2 and C_3H_5OH detection. In the case of NH_3 gas, no global maximum was observed below 200 °C.

Fig. 8 shows the results observed for three consecutive cycles of gas exposures of 10 ppm NH_3 and 2 ppm NO_2. The relative resistance change of the sensor follows a *p*-type semiconductor behavior, where the sensor's resistance increases due to the surface adsorption of electron-rich nucleophilic gas, NH_3, and decreases by the surface adsorption of electrophilic gas, NO_2 [32].

The Cu_2O sensor operates in synthetic air as the reference gas, so the adsorption of atmospheric oxygen leads to formation of a hole

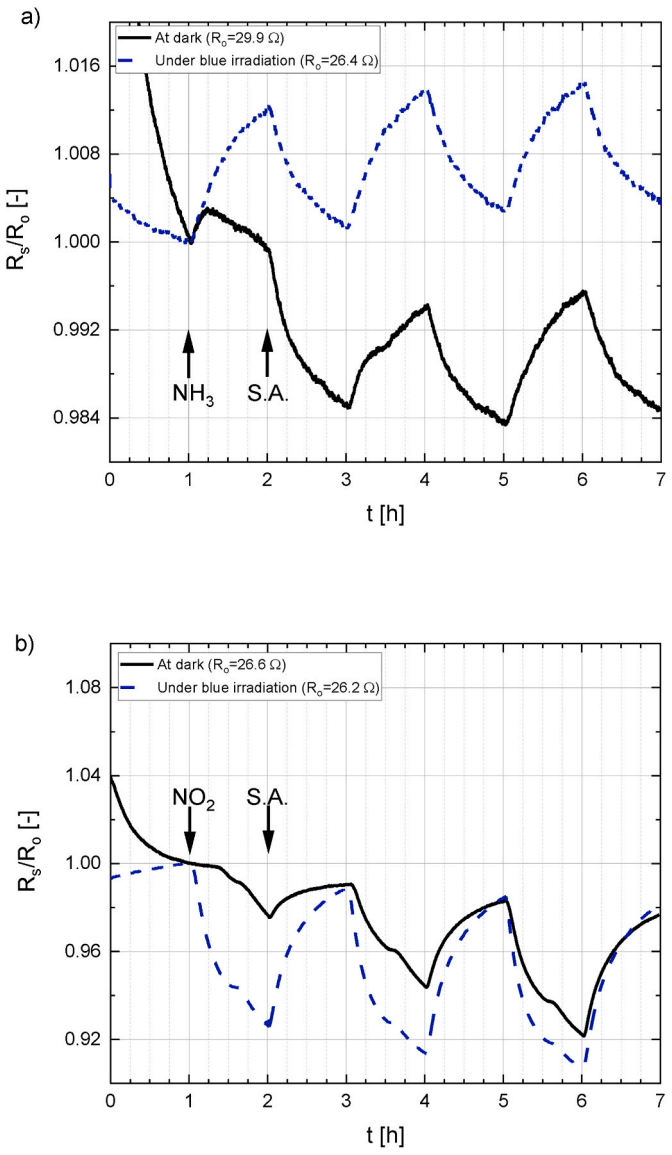

Fig. 8. Response of Cu_2O sensor in dark and blue light irradiation conditions for: a) 10 ppm NH_3 and b) 2 ppm NO_2 gas exposures.

accumulation layer (HAL) at the surface of the Cu_2O nanoparticles as depicted in Fig. 9. The adsorption of highly electrophilic (oxidizing) gases such as NO_2 causes electron trapping from the MOx valence band, increasing the HAL near the semiconductor surface, resulting in substantial band bending. The opposite takes place upon the adsorption of reducing molecules (NH_3). The band bending phenomena, therefore, promotes the charge transfer process, increasing the major carrier concentration, holes, while the measured resistance of the sensor decreases. On the other hand, when electron-rich nucleophilic NH_3 gas is chemisorbed, electrons are transferred to the MOx surface, thereby enhancing the recombination of electron-holes and HAL depletion. Consequently, the band bending decreases while the measured electrical resistance increases.

The plausible surface reactions occurring at the sensing layer with the adsorbed oxygen species can be described by the following reactions. The photo-excited electron in the conduction band reduces oxygen, viz.

$$O_{2\ (gas)} + e^- \rightarrow O^-_{2\ (adsorbed)}\ (T < 150^\circ C) \quad (1)$$

Upon light illumination, photon-induced oxygen adsorption occurs at the surface leading to an increase in the width of the HAL, thereby further faciliting adsorption/desoprtion process. The surface NO_2, NH_3, CH_2H_3OH gas adsorption mechanism on Cu_2O upon band gap illumination is described as follows:

$$Cu_2O + hv \leftrightarrow Cu_2O^* + e^- + h^+, \quad (2)$$

where Cu_2O^* is the excited state of Cu_2O.

NO_2 can also react with the excited conduction electron.

$$NO_{2\ (gas)} + e^- \rightarrow NO^-_{2\ (ads)} \quad (3)$$

In contrast, electrons are transferred to both ammonia and ethanol.

$$4NH_{3\ (gas)} + 5O^-_{2\ (ads.)} \rightarrow 6H_2O + 4NO_2 + 5e^- \quad (4)$$

$$C_2H_5OH\ (gas) + 3O^-_{2\ (ads.)} \rightarrow 3H_2O_{vap} + 2CO_{2\ (gas)} + 3e^- \quad (5)$$

A possible inhibition reaction 6 may however also occur for NO_2, whereby nitrates are formed which desorb only at elevated temperatures, well above 100 °C [33], viz.

$$3NO_{2,ads} + O^{2-}_{lattice} \rightarrow NO^-_{3,ads} + s\text{–}NO^-_3 + NO_{gas} \quad (6)$$

In reaction 6, NO_2 reacts with lattice O atoms to for surface bonded nitrates s–NO^-_3. The latter mechanism is strongly coverage dependent and at low NO_2 concentrations and oxygen excess nitrate formation is slow.

It can be seen in Fig. 8 that the gas sensing performance of the as-fabricated Cu_xO sensor films was significantly improved under blue light illumination. Furthermore, the sensor's response, recovery time, and stability were relatively enhanced for NH_3 and NO_2 gas exposures. The sensor responses can also determine two different time constants, as observed elsewhere [34]. The change of time constant of exponential sensor response is observed about 1 h after NO_2 or NH_3 exposures, visible as uneven exponential change that is most pronounced in the first cycle (Fig. 8). A possible explanation of the latter phenomenon could be NO_2 induced oxidation of the outermost CuO/Cu_4O_3 surface layer. Regardless of the mechanism, it is evident that the sensor drift and reproducible pulse shape more rapidly stabilize upon blue light illumination compared with dark operation conditions.

Finally, the sensitivity of the sensor was estimated. The sensors were exposed to reducing gas (NH_3) or oxidizing gas (NO_2) at fixed concentrations in five steps. The concentration was then increased every hour. The temperature was set according to the estimated optimal temperatures (150 °C at dark and 140 °C when irradiated by blue light). Before the measurements, the sensor was placed in synthetic air for two (NH_3) or three (NO_2) hours until it reached saturation. The results are presented in Figs. 10 and 11, respectively.

The sensor's detection limits (DL) towards NH_3 and NO_2 gases were computed using the polynomial approximation method described elsewhere [35,36]. Fig. 12 shows the DL extracted from the analysis using DC resistances, yielding high sensitivity with DL in the ppb regime. In particular, the DL was almost twice as low when the sample was irradiated by blue light as it was under dark conditions. The data shown in Figs. 10 and 11 exhibit some time drift and changes in the recorded DC resistance but consistently confirm the efficiency of the applied blue light illumination for gas sensing. Further studies are necessary to validate the DL of target analytes over a range of concentrations, including systematic studies of Cu_2O layer thickness, Cu_2O/Cu_4O_3 ratio, pulsed light operation, and optical power to optimize sensor performance further and elucidate operating mechanisms. For practical applications, further energy reduction can be accomplished by integrating the sensing layer with UV LED, e.g., by applying integrated circuits technology and reducing the distance between a light source and the sensing layer.

We considered irradiation by visible light of selected colors only because of its weighty effect on gas sensing, depending on the applied wavelengths. Other light sources (e.g., white light) will also improve gas

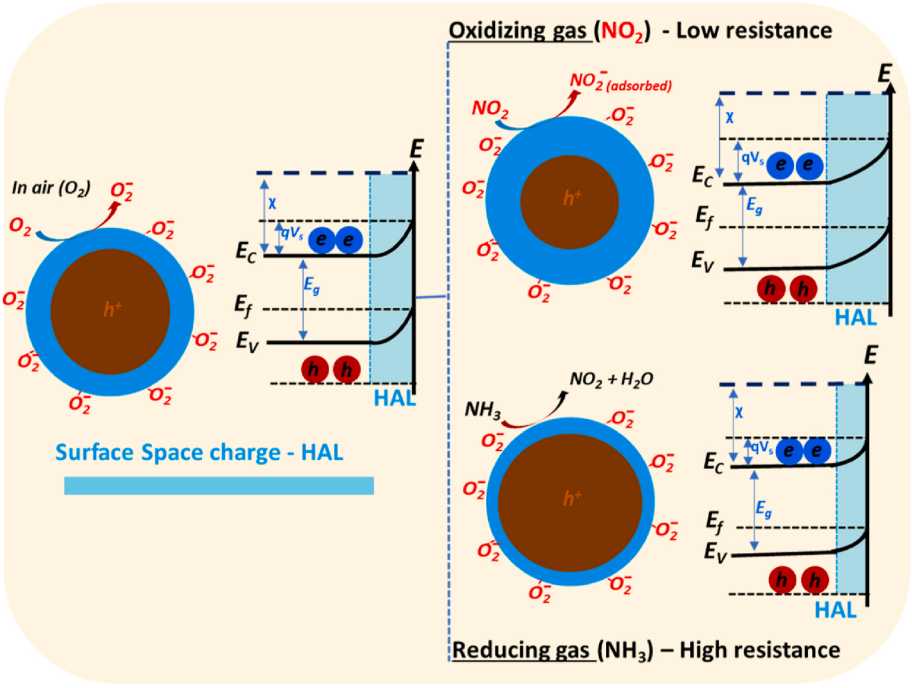

Fig. 9. Energy band diagram showing the HAL formation and band bending when Cu_2O sensor operates in the air or the presence of oxidizing (e.g. NO_2) or reducing (e.g. NH_3) gas. E_C, E_V, E_f and qV_s denote the conduction band, valence band, Fermi level, and surface potential, respectively.

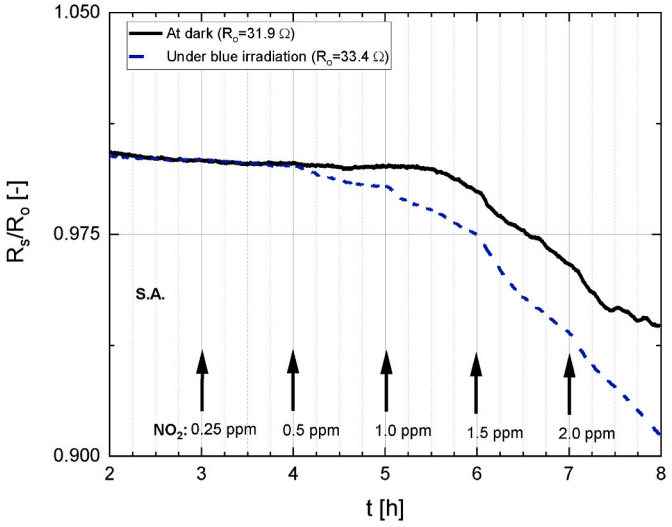

Fig. 10. Gas response of Cu_2O sensor to 0.25–2 ppm of NO_2 gas under dark (black solid line) and blue light (blue dashed line) conditions vs time *t*.

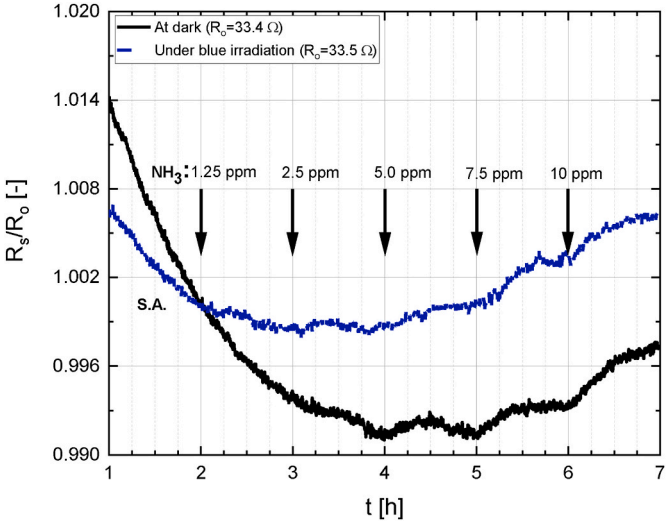

Fig. 11. Gas response of Cu_2O sensor to 1.25–10 ppm of NH_3 gas under dark (black solid line) and blue light (blue dashed line) conditions vs time.

sensitivity. Still, the lower impact of longer wavelengths on the gas sensing response due to the lower energy of irradiating photons requires more energy for the white light source than the most efficient blue light [37,38].

The presented result considers the impact of selected gases for electrophilic or nucleophilic on DC resistance of the studied gas sensing layer. We focused on the principal impact of these gases without considering the effects of the crossing interference of different gases, which must be considered in any practical applications. These effects require a selection of the interfering gases for the detailed studies because their presence at the surface of the sensing layer can induce chemical reactions or opposite changes of DC resistance, reducing gas sensitivity to the gas of interest and leading to new surface reactions. When considering a response to a mixture of two gases of opposite character (e.g., electrophilic NO_2, and nucleophilic NH_3) we observed a change in DC resistance induced by the gas of dominating character (higher bonding energy to sensor layer and higher induced DC response), and the sensitivity reduced by the interfering gas.

The reported detection limits (Fig. 12) suggest possible practical application in air quality monitoring, chemical process industries and medical application provided that the sensor response time and other sensor parameters are systematically optimized and calibrated with respect to each gas under study. We underline that the Cu_2O material is characterized by little influence of humidity variations, which is crucial in practical applications. Next, the measured dependence of the sensors' DC resistance on operating temperature for different gases under blue light irradiation (Figs. 6 and 7) provide further data that can be used for obtaining enhanced selectivity by a single gas sensor. The adequately

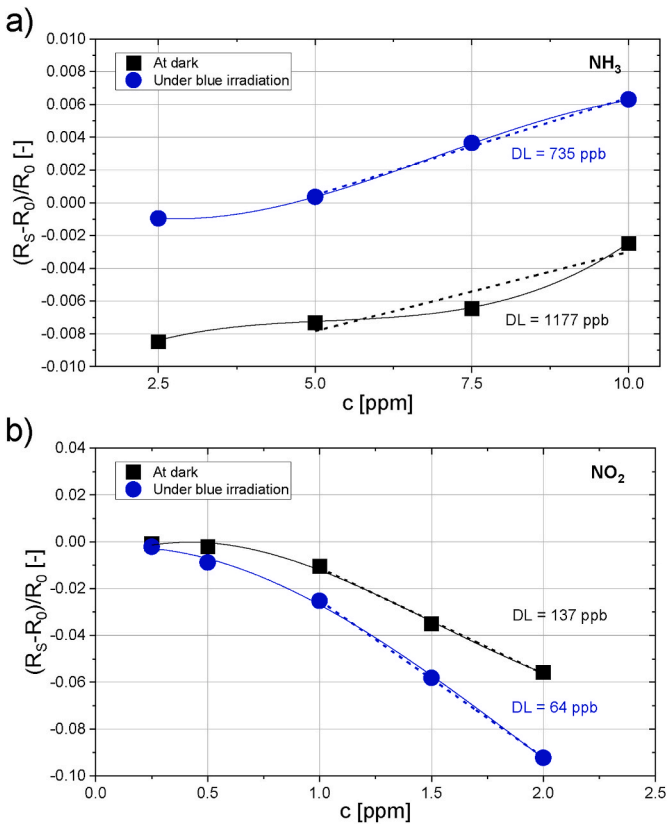

Fig. 12. Gas response calibration for Cu_2O sensor under dark conditions (black straight line) or blue light irradiation (blue straight line) at room temperature to gases: a) NH_3, b) NO_2 to determine the sensor's DL.

selected detection algorithms and short heating pulses, to modulate operating temperature, can further secure conditions for efficient gas sensing or reducing crossing gases effects.

4. Conclusions

We report on the fabrication and deposition of nanoporous copper oxide (Cu_2O) thin films employing a reactive advanced gas deposition technique. The as-fabricated thin films were characterized, and the film's corresponding surface morphology, structure, and composition depicted the deposition of highly nanoporous mixed copper oxides in Cu_2O and minor amounts of Cu_4O_3 phase at the surface. The gas sensing properties of the as-fabricated Cu_2O were characterized for two classes of gases: nucleophilic (ethanol and ammonia) and electrophilic (nitrogen dioxide), respectively. The gas sensing performance of the sensors was further characterized under dark and visible light conditions at different wavelengths. Thus, the sensors' responses to NO_2 and NH_3 gas exposures under blue light illumination demonstrated superior sensitivity even at room temperature. Moreover, blue light irradiation improves the repeatability and stability of the sensor's response. The results also suggest that the sensor's characteristic responses were mainly governed by chemical surface sensitization and surface electronic activation due to target adsorption and desorption processes under blue light illumination. The as-fabricated Cu_xO sensor films exhibit a relatively low detection limit of 64 ppb and 137 ppb for NO_2 and NH_3 gases, respectively. Finally, the nanoporous Cu_2O thin films demonstrated unique gas sensing features at relatively low operating temperatures toward reducing and oxidizing gases. Owing to its high porosity and low-temperature operation, the present *p*-type nanoporous Cu_2O sensor provided an interesting insight into the possibilities of selective gas sensing of oxidizing and reducing gases under visible light illumination. In the studied Cu_2O sensor, the dominant phase of Cu_2O is the main sensing material, but the outermost layer also contained Cu_4O_3 that may have influenced the interaction with the gas molecules, influencing the time constant of gas response. The impact of Cu_2O/Cu_4O_3 phase content in the surface region, and the interface between these layers, requires more detailed studies to determine optimal conditions for gas detection. The gas-sensing results of Cu_2O thin films towards selected gases of opposite properties under light irradiation further provided an insight into the catalytic and photon-induced sensing properties of highly nanoporous p-type copper oxide thin films. However, systematic and thorough studies are necessary for better understanding of the structure, morphology and thickness effects of the as-fabricated Cu_2O oxide. Cu_2O sensing layers were explored by others and presented similar results at low temperatures for NO_2 gas [39,40].

The observed response times to our test gases were relatively slow when considering practical applications. Such challenges are, however, inherent in most *p*-type MOx sensors, and this can be improved by applying different fabrication strategies and optimizations to control surface structure, morphology, and surface aspect ratio, or functionalizing with catalytic additives such as noble metal nanoparticles, oxide heterostructures, as well as modulating the surface catalytic and electronic sensitization under light irradiation. Additionally, we believe that noble metal nanoparticles can induce much better gas selectivity as observed in other gas-sensing materials and the presence of visible light irradiation [37,38].

CRediT authorship contribution statement

Andrzej Kwiatkowski: Writing – original draft, Software, Investigation. **Janusz Smulko:** Writing – review & editing, Funding acquisition, Conceptualization. **Katarzyna Drozdowska:** Visualization, Resources, Formal analysis. **Lars Österlund:** Writing – review & editing, Funding acquisition, Conceptualization. **Tesfalem Welearegay:** Writing – review & editing, Resources, Methodology, Investigation, Formal analysis, Conceptualization.

Declaration of competing interest

The authors declare that they have no known competing financial interests or personal relationships that could have appeared to influence the work reported in this paper.

Acknowledgment

This work was funded by the National Science Centre, Poland, under the research project 2019/35/B/ST7/02370, "System of gas detection by two-dimensional materials," and partially funded by the H2020-MSCA-RISE project "CanLeish" (grant no. 101007653).

References

[1] G. Giovannini, H. Haick, D. Garoli, Detecting COVID-19 from breath: a game changer for a big challenge, ACS Sens. 6 (2021) 1408–1417, https://doi.org/10.1021/acssensors.1c00312.
[2] C. Wang, L. Yin, L. Zhang, D. Xiang, R. Gao, Metal oxide gas sensors: sensitivity and influencing factors, Sensors 10 (2010) 2088–2106, https://doi.org/10.3390/s100302088.
[3] R. Ghosh, J.W. Gardner, P.K. Guha, Air pollution monitoring using near room temperature resistive gas sensors: a review, IEEE Trans. Electron. Dev. 66 (2019) 3254–3264, https://doi.org/10.1109/TED.2019.2924112.
[4] E. Llobet, Gas sensors using carbon nanomaterials: a review, Sens. Actuators, B 179 (2013) 32–45, https://doi.org/10.1016/j.snb.2012.11.014.
[5] D.R. Miller, S.A. Akbar, P.A. Morris, Nanoscale metal oxide-based heterojunctions for gas sensing: a review, Sens. Actuators, B 204 (2014) 250–272, https://doi.org/10.1016/j.snb.2014.07.074.
[6] Y. Chen, X. Zhang, Z. Liu, Z. Zeng, H. Zhao, X. Wang, J. Xu, Light enhanced room temperature resistive NO_2 sensor based on a gold-loaded organic–inorganic hybrid perovskite incorporating tin dioxide, Microchim. Acta 186 (2019) 1–10, https://doi.org/10.1007/s00604-018-3155-1.

[7] A.S. Chizhov, M.N. Rumyantseva, K.A. Drozdov, I.V. Krylov, M. Batuk, J. Hadermann, et al., Photoresistive gas sensor based on nanocrystalline ZnO sensitized with colloidal perovskite $CsPbBr_3$ nanocrystals, Sens. Actuators, B 329 (2021) 129035, https://doi.org/10.1016/j.snb.2020.129035.
[8] A. Singh, S. Sikarwar, A. Verma, B.C. Yadav, The recent development of metal oxide heterostructures based gas sensor, their future opportunities and challenges: a review, Sens. Actuators, B 332 (2021) 113127, https://doi.org/10.1016/j.sna.2021.113127.
[9] S. Ahmed, A. Ansari, M.A. Siddiqui, A. Khan, P. Ranjan, A potential optical sensor based on nanostructured silicon, J. Mater. Sci. Mater. Electron. 34 (2023) 755, https://doi.org/10.1007/s10854-023-10187-2.
[10] G.B. Smith, C.G. Granqvist, Green Nanotechnology: Solutions for Sustainability and Energy in the Built Environment, CRC Press, 2010.
[11] A. Depari, M. Falasconi, A. Flammini, D. Marioli, S. Rosa, G. SberveglieriG, et al., A new low-cost electronic system to manage resistive sensors for gas detection, IEEE Sensor. J. 7 (2007) 1073–1077, https://doi.org/10.1109/JSEN.2007.895965.
[12] E.L. Hines, E. Llobet, J.W. Gardner, Electronic noses: a review of signal processing techniques, IEE Proc. Circ. Dev. Syst. 146 (1999) 297–310, https://doi.org/10.1049/ip-cds:19990670.
[13] I. Polaka, M.P. Bhandari, L. Mezmale, L. Anarkulova, V. Veliks, A. Sivins, et al., Modular point-of-care breath analyzer and shape taxonomy-based machine learning for gastric cancer detection, Diagnostics 12 (2022) 491, https://doi.org/10.3390/diagnostics12020491.
[14] L. Zhang, D. Zhang, Efficient solutions for discreteness, drift, and disturbance (3D) in electronic olfaction, IEEE Trans. Syst. Man, Cybern. Syst 48 (2018) 242–254, https://doi.org/10.1109/TSMC.2016.2597800.
[15] C.N. Wang, Y.L. Li, F.L. Gong, Y.H. Zhang, S.M. Fang, H.L. Zhang, Advances in doped ZnO nanostructures for gas sensor, Chem. Rec. 20 (2020) 1553–1567, https://doi.org/10.1002/tcr.202000088.
[16] E.A.N. Simonetti, T.C. de Oliveira, Á.E. do Carmo Machado, A.A.C. Silva, A.S. dos Santos, L. de Simone Cividanes, TiO_2 as a gas sensor: the novel carbon structures and noble metals as new elements for enhancing sensitivity–a review, Ceram. Int. 47 (2021) 17844–17876, https://doi.org/10.1016/j.ceramint.2021.03.189.
[17] M. Penza, C. Martucci, G. Cassano, NO_x gas sensing characteristics of WO_3 thin films activated by noble metals (Pd, Pt, Au) layers, Sens. Actuators, B 50 (1998) 52–59, https://doi.org/10.1016/S0925-4005(98)00156-7.
[18] A. Mirzaei, H.R. Ansari, M. Shahbaz, J.Y. Kim, S.S. Kim, Metal oxide semiconductor nanostructure gas sensors with different morphologies, Chemosensors 10 (2022) 289, https://doi.org/10.3390/chemosensors10070289.
[19] T.P. Mokoena, H.C. Swart, D.E. Motaung, A review on recent progress of *p*-type nickel oxide based gas sensors: future perspectives, J. Alloys Compd. 805 (2019) 267–294, https://doi.org/10.1016/j.jallcom.2019.06.329.
[20] N. Rahman, J. Yang, M. Sohail, R. Khan, A. Iqbal, C. Maouche, A.A. Khan, M. Husain, S.A. Khattak, S.N. Khan, A. Khan, Insight into metallic oxide semiconductor (SnO_2, ZnO, CuO, α-Fe_2O_3, WO_3)-carbon nitride (g-C_3N_4) heterojunction for gas sensing application, Sens. Actuators, A 332 (2021) 113128, https://doi.org/10.1016/j.sna.2021.113128.
[21] M.R. Johan, M.S.M. Suan, N.L. Hawari, H.A. Ching, Annealing effects on the properties of copper oxide thin films prepared by chemical deposition, Int. J. Electrochem. Sci. 6 (2011) 6094–6104.
[22] S.J. Davarpanah, R. Karimian, F. Piri, Synthesis of copper (II) oxide (CuO) nanoparticles and its application as gas sensor, J. Appl. Biotechnol. Rep. 2 (2015) 329–332.
[23] https://www.tesla-blatna.cz. Multi-Sensor-Platform KBI2. https://www.tesla-blatna.cz/fe/files/senzory/datasheet_KBI2.pdf (accessed 2023-September-14).
[24] C.G. Granqvist, R.A. Buhrman, Ultrafine metal particles, J. Appl. Phys. 47 (1976) 2200, https://doi.org/10.1063/1.322870.
[25] T. Uyeda, C. Hayashi, A. Tasaki, Ultra-fine Particles: Exploratory Science and Technology, Elsevier, 1995.
[26] N. Fairley, V. Fernandez, M. Richard-Plouet, C. Guillot-Deudon, J. Walton, E. Smith, J. Baltrusaitis, Systematic and collaborative approach to problem solving using X-ray photoelectron spectroscopy, Appl. Surf. Sci. Adv. 5 (2021) 100112, https://doi.org/10.1016/j.apsadv.2021.100112.
[27] G. Greczynski, L. Hultman, X-ray photoelectron spectroscopy: towards reliable binding energy referencing, Prog. Mater. Sci. 107 (2020) 100591, https://doi.org/10.1016/j.pmatsci.2019.100591.
[28] J. Montero, L. Österlund, Photodegradation of stearic acid adsorbed on copper oxide heterojunction thin films prepared by magnetron sputtering, ChemEngineering 2 (2018) 40, https://doi.org/10.3390/chemengineering2030040.
[29] D.S. Murali, A. Subrahmanyam, Synthesis of low resistive *p*-type Cu_4O_3 thin films by DC reactive magnetron sputtering and conversion of Cu_4O_3 into CuO by laser irradiation, J. Phys. D Appl. Phys. 49 (2016) 375102, https://doi.org/10.1088/0022-3727/49/37/375102.
[30] Y. Wang, S. Lany, J. Ghanbaja, Y. Fagot-Revurat, Y.P. Chen, F. Soldera, D. Horwat, F. Mücklich, J.F. Pierson, Electronic structures of Cu_2O, Cu_4O_3, and CuO: a joint experimental and theoretical study, Phys. Rev. B 94 (2016) 245418, https://doi.org/10.1103/PhysRevB.94.245418.
[31] M.F. Al-Kuhaili, Characterization of copper oxide thin films deposited by the thermal evaporation of cuprous oxide (Cu_2O), Vacuum 82 (6) (2008) 623–629, https://doi.org/10.1016/j.vacuum.2007.10.004.
[32] C.E. Simion, B. Junker, U. Weimar, A. Stanoiu, N. Bârsan, Sensing mechanisms of CO and H_2 with NiO material–DRIFTS investigations, Sens. Actuators, B 390 (2023) 134028, https://doi.org/10.1016/j.snb.2023.134028.
[33] D. Langhammer, J. Kullgren, L. Österlund, Photo-adsorption and catalytic oxidation of NO_2 on anatase TiO_2: a combined dft and operando drift spectroscopy study, ACS Catal. 12 (2022) 10472–10481, https://doi.org/10.1021/acscatal.2c03334.
[34] G. Chaloeipote, R. Prathumwan, K. Subannajui, A. Wisitsoraat, C. Wongchoosuk, 3D printed CuO semiconducting gas sensor for ammonia detection at room temperature, Mater. Sci. Semicond. Process. 123 (2021) 105546, https://doi.org/10.1016/j.mssp.2020.105546.
[35] T. Pham, G. Li, E. Bekyarova, M.E. Itkis, A. Mulchandani, MoS_2-based optoelectronic gas sensor with sub-parts-per-billion limit of NO_2 gas detection, ACS Nano 13 (2019) 3196–3205, https://doi.org/10.1021/acsnano.8b08778.
[36] E. Desimoni, B. Brunetti, About estimating the limit of detection by the signal to noise approach, Pharm. Anal. Acta 6 (2015) 1–4, https://doi.org/10.4172/2153-2435.1000355.
[37] A. Chizhov, M. Rumyantseva, A. Gaskov, A. Light activation of nanocrystalline metal oxides for gas sensing: principles, achievements, challenges, Nanomaterials 11 (2021) 892, https://doi.org/10.3390/nano11040892.
[38] E. Espid, F. Taghipour, UV-LED photo-activated chemical gas sensors: a review, Crit. Rev. Solid State Mater. Sci. 42 (2017) 416–432, https://doi.org/10.1080/10408436.2016.1226161.
[39] H. Zhang, Q. Zhu, Y. Zhang, Y. Wang, L. Zhao, B. Yu, One-pot synthesis and hierarchical assembly of hollow Cu_2O microspheres with nanocrystals-composed porous multishell and their gas-sensing properties, Adv. Funct. Mater. 17 (2007) 2766–2771, https://doi.org/10.1002/adfm.200601146.
[40] L. Wang, R. Zhang, T. Zhou, Z. Lou, J. Deng, T. Zhang, Concave Cu_2O octahedral nanoparticles as an advanced sensing material for benzene (C_6H_6) and nitrogen dioxide (NO_2) detection, Sens. Actuators, B 223 (2016) 311–317, https://doi.org/10.1016/j.snb.2015.09.114.